Article

Cobalt-Containing Nitrogen-Doped Carbon Materials Derived from Saccharides as Efficient Electrocatalysts for Oxygen Reduction Reaction

Kaidi Veske [1], **Ave Sarapuu** [1,*], **Maike Käärik** [1], **Arvo Kikas** [2], **Vambola Kisand** [2], **Helle-Mai Piirsoo** [2], **Alexey Treshchalov** [2], **Jaan Leis** [1], **Aile Tamm** [2] and **Kaido Tammeveski** [1]

[1] Institute of Chemistry, University of Tartu, Ravila 14a, 50411 Tartu, Estonia; kaidiveske@gmail.com (K.V.); maike.kaarik@ut.ee (M.K.); jaan.leis@ut.ee (J.L.); kaido.tammeveski@ut.ee (K.T.)

[2] Institute of Physics, University of Tartu, W. Ostwald Str. 1, 50411 Tartu, Estonia; arvo.kikas@ut.ee (A.K.); vambola.kisand@ut.ee (V.K.); helle-mai.piirsoo@ut.ee (H.-M.P.); aleksei.trestsalov@ut.ee (A.T.); aile.tamm@ut.ee (A.T.)

* Correspondence: ave.sarapuu@ut.ee

Abstract: The development of non-precious metal electrocatalysts towards oxygen reduction reaction (ORR) is crucial for the commercialisation of polymer electrolyte fuel cells. In this work, cobalt-containing nitrogen-doped porous carbon materials were prepared by a pyrolysis of mixtures of saccharides, cobalt nitrate and dicyandiamide, which acts as a precursor for reactive carbon nitride template and a nitrogen source. The rotating disk electrode (RDE) experiments in 0.1 M KOH solution showed that the glucose-derived material with optimised cobalt content had excellent ORR activity, which was comparable to that of 20 wt% Pt/C catalyst. In addition, the catalyst exhibited high tolerance to methanol, good stability in short-time potential cycling test and low peroxide yield. The materials derived from xylan, xylose and cyclodextrin displayed similar activities, indicating that various saccharides can be used as inexpensive and sustainable precursors to synthesise active catalyst materials for anion exchange membrane fuel cells.

Keywords: electrocatalysis; oxygen reduction reaction; non-precious metal catalyst; MNC catalyst; carbon nitride template

1. Introduction

Low-temperature fuel cells are promising devices for converting H_2 generated from renewable energy back to electricity. Among these, proton exchange membrane fuel cells (PEMFCs) have already found commercial application in the transport sector; however, they rely on high-cost catalysts containing platinum-group metals (PGM) [1]. Anion exchange membrane fuel cell (AEMFC) technology allows using cheaper materials, including non-precious metal catalysts, and their performance has been significantly improved in recent years [2–5]. The United States Department of Energy has set a target to reach PGM-free AEMFCs by 2030 [6]. Thus, it is necessary to develop high-performance PGM-free catalysts for both O_2 reduction reaction (ORR) occurring in fuel cell cathode and hydrogen oxidation reaction on anode.

The PGM-free catalysts for ORR have been intensely developed in recent decades, and among these, transition metal-containing nitrogen-doped carbon (MNC) catalysts have shown the most promising results [1,4,7–11]. These catalysts can be synthesised from existing carbon precursors such as carbon black [12], carbon nanotubes (CNTs) [13], carbide-derived carbon (CDC) [14], CNT–CDC composites [15,16], mesoporous carbon [17,18], graphene [19], natural shungite [20], etc., by doping the surface of these materials in high-temperature pyrolysis with nitrogen and transition metal sources. Alternatively, it is possible to synthesise the nanocarbons by pyrolysing organic precursors while simultaneously doping these with nitrogen and transition metal [21–27]. This is a cost-effective

approach, as besides simple organic compounds, any organic biomass, such as agricultural waste products, can be used as carbon precursors [28,29]. Glucose as one of the simplest and easily producible organic compounds has been a popular choice for carbon precursor and has often been used in the preparation of ORR catalysts [30–33], but other carbohydrates have also been employed [34–36]. However, when synthesising the carbon catalysts from organic precursors, one of the main challenges is to achieve a porous structure suitable for the fuel cell application, preferentially hierarchical porosity. The most common methods to tailor the porous structure is using hard or soft templates [37]. It has been shown that graphitic carbon nitride (g-C_3N_4), which forms from some simple N sources, such as dicyandiamide (DCDA), urea or melamine during the pyrolysis at about 550–600 °C, can also serve as a template in the synthesis of N-doped carbon materials [22,23,30,33,35,36,38,39]. It decomposes when the temperature is further increased, and the nitrogen-containing gases are released that act as dopants of the carbon material [33,35].

In addition to favourable morphology, the high-performing carbon-based catalysts should have a high number density of ORR-active sites. In alkaline solution, these can be either various metal-free nitrogen-containing functionalities (pyridinic-N, pyrrolic-N, graphitic-N, etc.), nitrogen-coordinated single-atom transition metal centres (M-N_x), or metal-containing nanoparticles, such as carbides, oxides, nitrides, or metals, which are often encased by carbon layers [10,40]. The catalysts prepared by pyrolysis contain many of these centres and despite numerous efforts, the exact mechanism of the ORR has not been revealed as yet. It is very likely that all such sites are involved in the ORR process, and in some works, synergetic effects between these have been also proposed [41–43].

Previously, we have successfully used the carbon nitride template-based approach to synthesise PGM-free ORR catalysts from 5-methylresorcinol [22,23]. In this work, saccharides were employed as cheap and sustainable organic precursors to prepare cobalt-containing N-doped carbon catalysts by simple one-step high-temperature pyrolysis. High electrocatalytic activity for ORR in 0.1 M KOH solution was demonstrated by the rotating disk electrode (RDE) method and the dependence of the catalyst performance on the cobalt content was revealed. The ORR activity of the catalysts did not depend on the nature of the saccharide employed; thus, this work provides a feasible route towards the production of sustainable and cost-effective cathode materials for the AEMFC application.

2. Results and Discussion

2.1. Structural Characterisation

The cobalt-containing N-doped carbon catalysts Glu-NC-Co, Glu-NC-4Co, Glu-NC-8Co and Glu-NC-16Co were prepared by pyrolysis of the mixture of glucose, dicyandiamide and various amounts of $Co(NO_3)_2 \cdot 6H_2O$. The scanning electron microscopy (SEM) studies of surface morphology of Glu-NC-8Co reveal that pyrolysis of the mixture of carbon, nitrogen and cobalt precursors results in a porous carbon material with irregular structure and a network of interconnected meso- and macropores (Figure 1). It has been proposed that during the pyrolysis, DCDA forms g-C_3N_4 nanosheets at ca. 550 °C, which act as an in situ template for the formation of carbon nanosheets from glucose and yields a high mesoporosity of the resulting material [30]. By increasing the temperature of pyrolysis over 600 °C, g-C_3N_4 starts to decompose to reactive gases, such as NH_3 and CO_2, which induce additional porosity and introduce N-containing active sites to the catalyst [33,35]. According to energy-dispersive X-ray spectroscopy (EDX) results, the catalyst material contained 24 wt% Co, 61 wt% C, 8 wt% of N and 7 wt% of O. Since the metal content is rather high, it is expected that the material also contains cobalt-rich nanoparticles encapsulated in carbon layers, as shown in the previous reports on the materials prepared by similar approach [22,31,34].
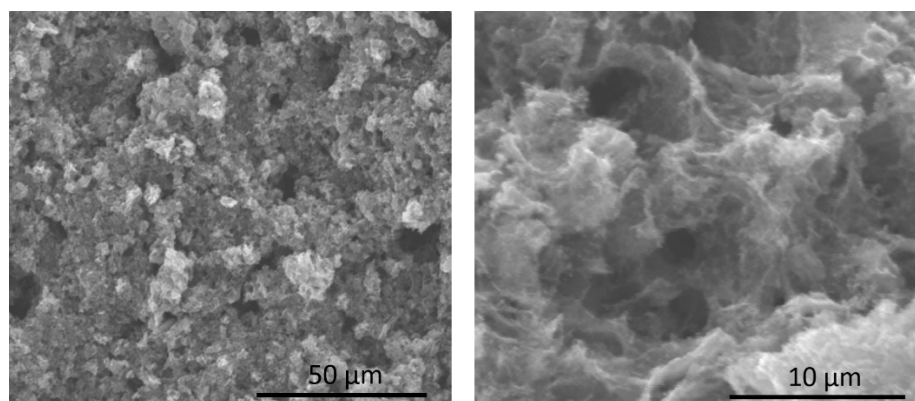
Figure 1. Scanning electron microscopy images of the Glu-NC-8Co catalyst material.

N$_2$ physisorption analysis was performed to examine the specific surface area and porosity of the catalyst material. The N$_2$ adsorption/desorption isotherm of Glu-NC-8Co (Figure 2a inset) corresponds to the type III isotherm with the H4 hysteresis loop according to the IUPAC classification [44], which is characteristic of micro-mesoporous materials with a low content of micropores. The specific surface area (S_{BET}) was 275 m^2 g^{-1} and the total pore volume was 0.39 cm^3 g^{-1}, of which 0.07 cm^3 g^{-1} was the micropore volume. In the pore size distribution graph (Figure 2a), the maximum is at about 3.5 nm, and it can be seen that most of the pores are less than 6 nm in diameter; however, there are also some larger mesopores of various size present in the material. Such hierarchical porosity is beneficial for the fuel cell catalysts, as the existence of mesopores is required for enhancing the mass transfer of the reactants and products in the catalyst layer and high microporosity ensures a high number of ORR-active sites [45].
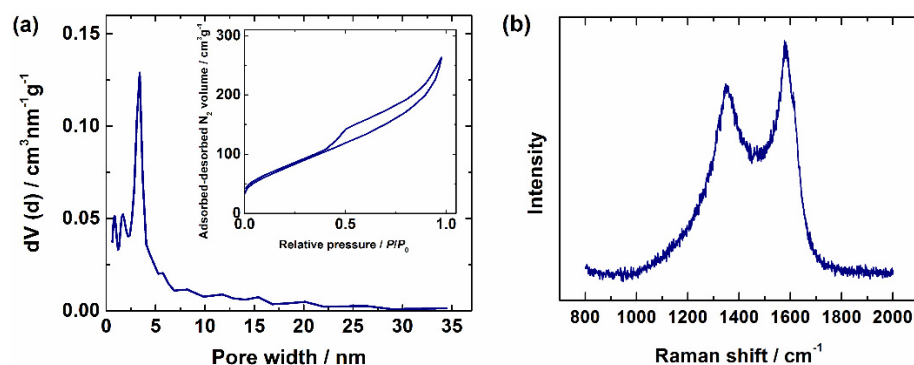

Figure 2. (**a**) Pore size distribution curve and N$_2$ physisorption isotherm (inset) for Glu-NC-8Co material. (**b**) Raman spectrum of Glu-NC-8Co catalyst.

The results of Raman spectroscopy (Figure 2b) provide information on the structure of Glu-NC-8Co carbon material. The D-band (at ca. 1350 cm^{-1}) is associated with the defects and disorder in the carbon structure, while the G-band (at ca. 1580 cm^{-1}) corresponds to the regular crystalline graphitic carbon. The highly broadened and intense D band indicates that the material has a rather defective and irregular structure, which is characteristic for the doped carbon. However, a rather intense G-peak suggests the sufficient graphitisation of the material, which has been shown to be promoted by transition metals [46] and is necessary to provide good electrical conductivity to the material.

X-ray photoelectron spectroscopy (XPS) analysis was performed to examine the elemental content of the catalyst surface (Figure 3). The Glu-NC-8Co material was found to contain 9.1 at % N, 2.5 at % Co, 81.6 at % C and 6.8 at % O. Figure 3b shows the detailed XPS spectrum in the N 1s region, deconvoluted into components corresponding to different functional groups in the material. According to the peak fitting, the material contains the highest amount of pyridinic N (43% of the total nitrogen content, peak at 398.5 eV);

the other peaks can be assigned to metal-coordinated N (399.5 eV, 15%), hydrogenated N (including pyrrolic N and hydrogenated pyridine [47], 400.6 eV, 25%), graphitic N (402.0 eV, 10%), N-H (403.7 eV, 4%) and N-O (405.2 eV, 2%). Previous studies have shown that pyridinic and metal-coordinated nitrogen moieties have the highest electrocatalytic activity towards the ORR in alkaline solution [25]. The detailed Co 2p spectrum (Figure 3a, inset) consists of multiple peaks corresponding to oxidised forms of Co, which could be metal oxides but also N-coordinated single-atom centres. The identification of these peaks is not possible, because they consist of multiple overlapping peaks due to multiplet splitting and charge transfer effects [48]. The small peak at the lowest binding energy (778.1 eV) can be assigned to metallic Co, which corresponds to about 2% of total surface cobalt. The deconvolution of detailed O 1s and C 1s photoelectron spectra (Figure 3c,d) reveals that there are various functional groups on the surface. The subpeaks can be attributed to O in carbonyl (531.2 eV); ether/alcohol/-C=O in ester (531.5 eV) and –OH in carboxyl/-C-O-C in ester (532.9 eV) [49]; the subpeak with the lowest binding energy (530.3 eV) can be related to metal oxides. The C 1s peak consists of components corresponding to sp^2 and sp^3 carbon (284.7 and 285.5 eV, respectively) and several peaks that can be attributed to various functional groups with C-O and C-N bonds [49,50].
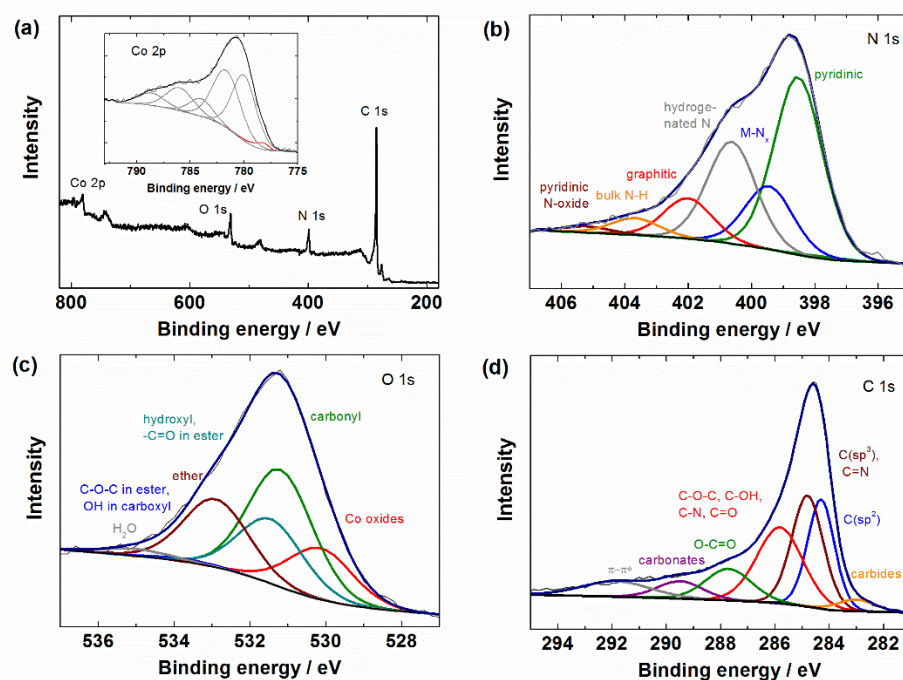

Figure 3. X-ray photoelectron spectra for Glu-NC-8Co catalyst: survey spectrum (**a**) and deconvoluted detailed spectra in Co 2p region (inset of (**a**)), N 1s region (**b**), O 1s region (**c**) and C 1s region (**d**).

2.2. Electrochemical Characterisation

The electrocatalytic activity of carbon-based catalyst materials was studied using the rotating disk electrode method (RDE) in 0.1 M KOH saturated with O_2. The metal content in the catalyst was varied to achieve the maximum activity. The comparison of RDE polarisation curves in Figure 4a shows that the electrocatalytic activity of Co-containing materials was considerably higher than that of cobalt-free catalyst (Glu-NC), and the activity increased with increasing the metal content. The most positive value of the half-wave potential ($E_{1/2}$) of −0.18 V vs. saturated calomel electrode (SCE) was achieved with Glu-NC-8Co and two times higher metal content (Glu-NC-16Co) did not further improve this, although Glu-NC-16Co showed slightly higher onset potential (E_{onset}, corresponds to the potential at which the ORR current density reaches the value of −0.1 mA cm^{-2}) of −0.04 V (Table 1). It can also be seen that the electrocatalytic activity of these catalysts is equal to that of commercial Pt/C catalyst. The catalyst Glu-NC-8Co was treated in acid to obtain

the material Glu-NC-8Co-at, but this did not have a positive effect on the ORR activity of the catalyst, as the values of $E_{1/2}$ and E_{onset} were slightly more negative for Glu-NC-8Co-at material as compared to Glu-NC-8Co. Although dissolving the metal-rich nanoparticles is necessary to increase the ORR activity of MNC catalysts in acidic solution [51], the effect of it to the electrocatalytic activity in alkaline media is controversial, as these can contribute to the activity of the materials, and the removal of these can decrease the ORR activity [34,39].
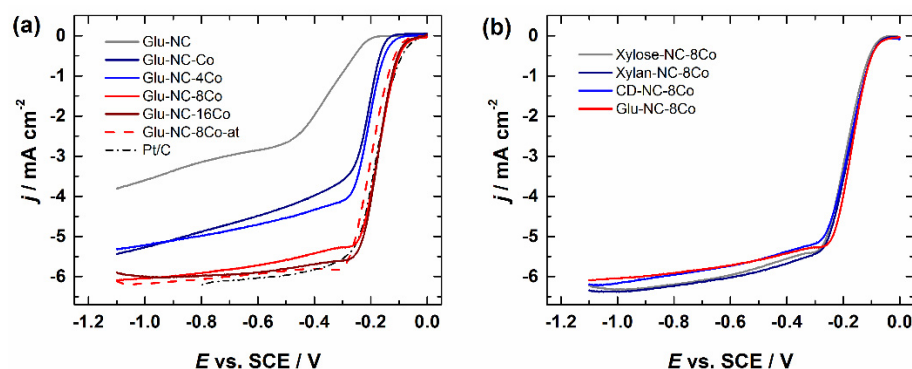

Figure 4. RDE voltammetry curves of O_2 reduction in O_2-saturated 0.1 M KOH on (**a**) glucose-derived catalyst materials and Pt/C; (**b**) catalysts derived from various saccharides. ω = 1900 rpm, v = 10 mV s^{-1}.

Table 1. ORR parameters of the electrocatalysts in 0.1 M KOH solution.

Catalyst	$E_{1/2}$ (V vs. SCE)	E_{onset} (V vs. SCE)	n (at -1.1 V)
Glu-NC	-0.40	-0.21	3.2
Glu-NC-Co	-0.24	-0.14	4.0
Glu-NC-4Co	-0.22	-0.11	4.0
Glu-NC-8Co	-0.18	-0.06	4.3
Glu-NC-16Co	-0.18	-0.04	4.1
Glu-NC-8Co-at	-0.20	-0.07	4.1
Xylan-NC-8Co	-0.19	-0.07	4.0
Xylose-NC-8Co	-0.20	-0.07	4.1
CD-NC-8Co	-0.19	-0.07	4.2
Pt/C	-0.18	-0.04	3.9

To evaluate the applicability of the synthesis method for other carbohydrates, saccharides with different structures were used as organic precursors instead of glucose: xylose, xylan, and cyclodextrin to obtain the catalyst materials Xylose-NC-8Co, Xylan-NC-8Co and CD-NC-8Co, respectively. It can be seen from Figure 4b and Table 1 that the values of E_{onset} and $E_{1/2}$ of the O_2 reduction for the materials prepared from different saccharides are rather similar to that of Glu-NC-8Co. Thus, it can be assumed that this synthesis method is universal for the preparation of MNC catalysts from saccharides.

To further investigate the ORR pathway on the catalysts, the RDE polarisation curves were recorded at different electrode rotation rates (Figure 5a), and the number of electrons transferred (n) was found from the Koutecky–Levich equation [52]:

$$\frac{1}{j} = \frac{1}{j_k} + \frac{1}{j_d} = -\frac{1}{nFkc^b_{O_2}} - \frac{1}{0.62nFD^{2/3}_{O_2}v^{-1/6}c^b_{O_2}\omega^{1/2}} \tag{1}$$

where j is the experimental current density, j_k is the kinetic current density, j_d is the diffusion-limited current density, n is the number of electrons transferred per O_2 molecule, k is the O_2 reduction rate constant (cm s^{-1}), F is the Faraday constant (96,485 C mol^{-1}), D_{O_2} is the diffusion coefficient of oxygen (1.9×10^{-5} cm^2 s^{-1}) [53], v is the kinematic viscosity of the solution (0.01 cm^2 s^{-1}) [54], $c^b_{O_2}$ is the concentration of oxygen in the bulk solution (1.2×10^{-6} mol cm^{-3}) [53] and ω is the electrode rotation rate (rad s^{-1}). Figure 5b shows

the Koutecky–Levich plots for the Glu-NC-8Co material at different potentials and the value of n calculated from the slopes of these, which is close to four over the whole range of potentials studied. Thus, it can be concluded that the final product of O_2 reduction is OH^-. Similarly, a $4e^-$ reduction in O_2 was confirmed for all catalysts (Table 1), except for the metal-free Glu-NC, on which a lower n value suggests partial $2e^-$ reduction to hydroperoxide anion (HO_2^-).
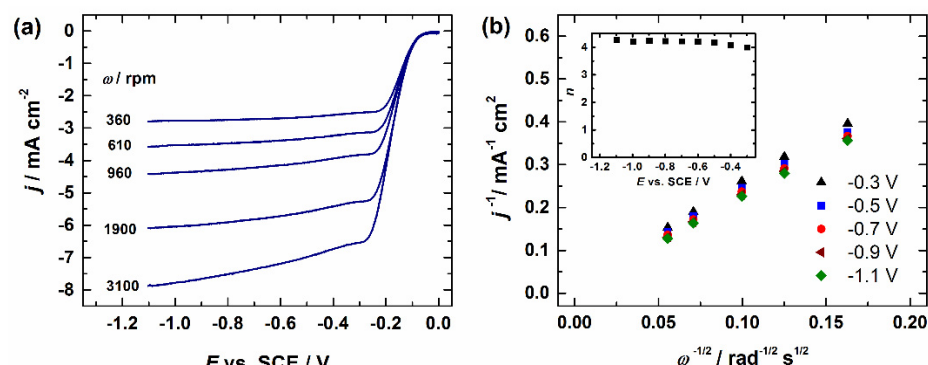

Figure 5. (**a**) RDE voltammetry curves of O_2 reduction on Glu-NC-8Co catalyst in O_2-saturated 0.1 M KOH, $\nu = 10$ mV s^{-1}; (**b**) Koutecky–Levich plots derived from data in (**a**) and number of electrons transferred (inset).

A comparison of the catalysts with different metal content (Figure 4a) indicates that the presence of sufficient amount of cobalt salt in the carbonisation process is necessary to obtain active ORR electrocatalysts. However, it is expected that many different cobalt- and nitrogen-containing species form during the pyrolysis, and the exact role of these in ORR electrocatalysis is not clear. The nitrogen-coordinated single-atom transition metal centres (MN_x) are shown to be active sites for the ORR [25,43,55–59]; however, in alkaline media, a high activity of metal-containing nanoparticles has also been demonstrated [39,41,43,60,61]. Therefore, increasing the catalysts' activity with increasing cobalt content is an expected result, as the number of electroactive centres is also expected to increase. On the other hand, cobalt is known to promote graphitisation of the carbon material formed during the pyrolysis [46]; thus, the higher metal content may increase the conductivity of the materials, which is also beneficial to the activity.

In order to indirectly show the existence of $M-N_x$ centres in the catalyst and their role in the ORR process, the effect of cyanide anions to the O_2 reduction activity was determined. Cyanide ions are known to bind irreversibly to $M-N_x$ centres and block the access of these sites to O_2 molecules, thereby inhibiting the ORR rate on the MNC catalysts [12,62]. It can be seen from Figure 6a that the electrocatalytic activity was significantly reduced in the presence of CN^-, with E_{onset} decreasing by 0.11 V and $E_{1/2}$ by 0.09 V. Thus, it can be concluded that Glu-NC-8Co catalyst contains $M-N_x$ centres, and these have a large contribution to their ORR activity. The remaining ORR activity is presumably related to O_2 reduction on metal-free N centres, such as pyridinic N and graphitic N, and possibly on cobalt-containing nanoparticles surrounded by an N-doped carbon shell.
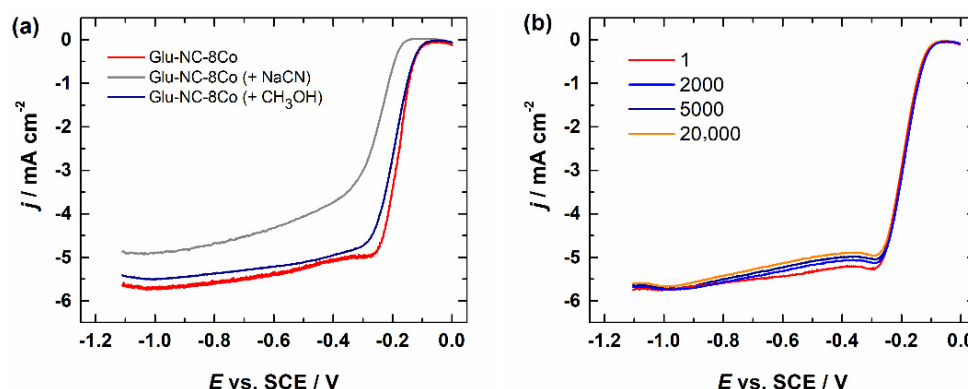
Figure 6. RDE voltammetry curves for O_2 reduction on Glu-NC-8Co catalyst in O_2-saturated 0.1 M KOH (**a**) in the presence of 10 mM NaCN or 3 M methanol, (**b**) before and after a certain number of potential cycles between 0 and -0.4 V. ω = 1900 rpm, ν = 10 mV s^{-1}.

To assess the methanol tolerance of the catalyst, the electrocatalytic activity of O_2 reduction was determined in the presence of 3 M of methanol. It can be seen from Figure 6a that methanol had very little effect on the RDE polarisation curves, so it can be concluded that the material has a high methanol tolerance and therefore could also be a suitable cathode catalyst for direct methanol fuel cells.

The stability of the catalyst materials is an important characteristic for the application in the low-temperature fuel cells. As compared to PGM-based materials, non-PGM catalysts show higher durability in AEMFCs [3]. A short-term stability test was performed with Glu-NC-8Co, in which 20,000 potential cycles were applied and O_2 reduction polarisation curves were recorded after a certain number of cycles (Figure 6b). It can be seen that the ORR current gradually decreased in the intermediate potential range from -0.3 to -0.9 V vs. SCE, but it remained rather stable in the kinetic region and at more negative potentials. There was only a negligible decrease in the values of E_{onset} and $E_{1/2}$ after the potential cycling. Hence, this catalyst can be considered as rather stable in alkaline environment.

3. Materials and Methods

3.1. Preparation of Catalyst Materials

For the preparation of catalysts, 0.15 g of D-glucose (Sigma-Aldrich, St. Louis, MO, USA), 1.5 g of dicyandiamide (DCDA, Sigma-Aldrich) and 0.01–0.16 g of Co(NO$_3$)$_2$·6H$_2$O (Sigma-Aldrich) were dissolved in the mixture of 10 mL of 2-propanol and 20 mL of Milli-Q water and sonicated for about 30 min. The solution was dried at 35 °C overnight, and the dried precursor mixture was pyrolysed at 800 °C for 2 h in N$_2$ atmosphere, raising the temperature by the ramp rate of 10 °C min^{-1}. The materials prepared using 0.01 g, 0.04 g, 0.08 g and 0.16 g of Co salt are designated as Glu-NC-Co, Glu-NC-4Co, Glu-NC-8Co and Glu-NC-16Co, respectively. For comparison, a metal-free material (Glu-NC) was prepared similarly but without Co salt. The catalyst materials were also prepared by replacing glucose with xylan (Sigma-Aldrich), D-xylose (Sigma-Aldrich) and β-cyclodextrin (Sigma-Aldrich), denoted as Xylan-NC-8Co, Xylose-NC-8Co and CD-NC-8Co, respectively. Glu-NC-8Co material was also acid-treated in the aqueous solution of 0.5 M HNO$_3$ (Sigma-Aldrich) and 0.5 M H$_2$SO$_4$ (Sigma-Aldrich) at 50 °C for 8 h; then, it was filtered, rinsed with water, dried and pyrolysed again at 800 °C for 2 h to obtain the material Glu-NC-8Co-at.

3.2. Electrochemical Measurements

Glassy carbon (GC) electrodes with a geometric area of 0.2 cm^2 were used for electrochemical measurements by the rotating disk electrode method. The surface of the GC electrodes was polished with 1 and 0.3 μm particle diameter alumina powder (Buehler, Uzwil, Switzerland), sonicated first in Milli-Q water and then in 2-propanol for about 5 min. Then, 4 mg of catalyst was dispersed in the mixture of 653 μL of 2-propanol, 327 μL of water and 20 μL of a 5% solution of Nafion (Sigma-Aldrich) by sonication for 30 min. The

GC electrode was drop-coated with two 5 μL aliquots of the suspension to yield the catalyst loading of 200 μg cm^{-2}. For comparison, a commercial Pt/C catalyst (20 wt%, E-TEK, BASF Fuel Cell, Somerset, NJ, USA) was applied by the same method, resulting in the final Pt loading of 40 μg$_{Pt}$ cm^{-2} on the electrode.

Electrochemical oxygen reduction was studied with the RDE method in 0.1 M KOH aqueous solution prepared from KOH pellets (Sigma-Aldrich), saturated with oxygen (99.999%, Linde, Dublin, Ireland), using an EDI101 rotator (Radiometer, Copenhagen, Denmark), CTV101 speed controller (Radiometer) and an Autolab potentiostat/galvanostat PGSTAT30 (Metrohm-Autolab, Utrecht, The Netherlands). The reference electrode was a saturated calomel electrode (SCE), and the auxiliary electrode was a carbon rod. The background currents recorded in the electrolyte solution saturated with argon (99.999%, Linde) were subtracted from the corresponding RDE polarisation data. The methanol tolerance of the catalysts was studied in 3 M solution of methanol in 0.1 M KOH. To study the effect of cyanide anions, the ORR experiments were conducted in the presence of 10 mM NaCN (Sigma-Aldrich) in 0.1 M KOH solution. The short-time stability tests were performed by cycling the potential between −0.5 and 0 V for 20,000 potential cycles at a scan rate (ν) of 200 mV s^{-1}, and the RDE polarisation curves for oxygen reduction were measured after 2000, 5000, and 20,000 potential cycles.

3.3. Physicochemical Characterisation

SEM with EDX was used to study and characterise the surface morphology and composition of the Glu-NC-8Co material. The GC disk was drop-coated with the catalyst material, and the measurements were performed with a Helios Nanolab 600 (FEI, Hillsboro, OR, USA) electron microscope attached INCA Energy 350 (Oxford Instruments, Abingdon, UK) spectrometer.

The N$_2$ adsorption/desorption isotherms were recorded on a NovaTouch LX2 (Quantachrome Instruments, Boynton Beach, FL, USA) at the boiling point of N$_2$ (77 K). The sample was degassed in vacuum at 300 °C for 12 h before measurements. The S_{BET} was calculated according to the Brunauer–Emmett–Teller (BET) theory. The total pore volume was measured at $P/P_0 = 0.97$. The micropore volume and pore size distribution were calculated using quenched solid density functional theory (QSDFT) equilibria model for slit-type pores. TouchWin 1.11 software (Quantachrome Instruments) was used for calculations.

For the Micro-Raman spectroscopic analysis, the catalyst suspension was pipetted onto a Si plate. The spectrum was recorded on an inVia Raman spectrometer (Renishaw, Wotton-under-Edge, UK) with an Ar ion laser operating at 514.5 nm and a confocal microscope (Leica Microsystems, Mannheim, Germany) with 50X objective.

The XPS analysis was conducted with a SCIENTA SES-100 electron energy analyser (VG Scienta, Uppsala, Sweden) and a non-monochromatic twin anode X-ray source Thermo XR3E2 (Thermo Fisher Scientific, Waltham, MA, USA). The Mg K$_\alpha$ X-rays with photon energy 1253.6 eV were used. The survey spectrum was registered in the range of 1000 to 0 eV with a pass energy of 200 eV, step size of 0.5 eV, step duration of 0.2 s and number of scans: 5. For collecting the detailed spectra, the step size of 0.2 eV, step duration of 0.2 s and the number of scans of at least 25 were used. The data were processed with Casa-XPS software (version 2.3.17, Casa Software, Teignmouth, UK); this included removing X-ray satellites. The peak fitting was completed using a Gauss–Lorentz hybrid function (GL 70, Gauss 30 %, Lorentz 70 %) and a blend of linear and Shirley-type backgrounds.

4. Conclusions

Cobalt-containing nitrogen-doped carbon-based catalyst materials for the ORR were prepared by the pyrolysis of saccharides in the presence of cobalt salt and dicyandiamide as a nitrogen precursor. Graphitic carbon nitride formed in situ during the pyrolysis acted as a reactive template to yield porous materials. In the rotating disk electrode experiments, the material with optimised cobalt content had a remarkably high ORR activity in alkaline solution, which was comparable to that of a 20 wt% Pt/C catalyst.

The catalyst materials prepared from glucose, xylose, xylan and cyclodextrin had similar activity; thus, it is expected that this synthesis method can be applied to any saccharides. Acid treatment of the catalyst did not increase its electrocatalytic activity. The number of electrons transferred was found to be around 4 for all Co-containing catalysts. Glu-NC-8Co catalyst was stable during potential cycling for 20,000 cycles and had a high methanol tolerance. In the presence of cyanide anions, the electrocatalytic activity of Glu-NC-8Co decreased significantly, indicating that the catalyst contains M-N_x as active centres.

This work provides a simple procedure to prepare active and stable non-precious metal catalyst materials for AEMFC cathodes, starting from inexpensive and abundant precursors.

Conflicts of Interest: The authors declare no conflict of interest.

References

1.   He, Y.H.; Liu, S.W.; Priest, C.; Shi, Q.R.; Wu, G. Atomically dispersed metal-nitrogen-carbon catalysts for fuel cells: Advances in catalyst design, electrode performance, and durability improvement. *Chem. Soc. Rev.* **2020**, *49*, 3484–3524. [CrossRef] [PubMed]
2.   Dekel, D.R. Review of cell performance in anion exchange membrane fuel cells. *J. Power Sources* **2018**, *375*, 158–169. [CrossRef]
3.   Firouzjaie, H.A.; Mustain, W.E. Catalytic Advantages, Challenges, and Priorities in Alkaline Membrane Fuel Cells. *ACS Catal.* **2020**, *10*, 225–234. [CrossRef]
4.   Sarapuu, A.; Kibena-Põldsepp, E.; Borghei, M.; Tammeveski, K. Electrocatalysis of oxygen reduction on heteroatom-doped nanocarbons and transition metal-nitrogen-carbon catalysts for alkaline membrane fuel cells. *J. Mater. Chem. A* **2018**, *6*, 776–804. [CrossRef]
5.   Ramaswamy, N.; Mukerjee, S. Alkaline Anion-Exchange Membrane Fuel Cells: Challenges in Electrocatalysis and Interfacial Charge Transfer. *Chem. Rev.* **2019**, *119*, 11945–11979. [CrossRef] [PubMed]
6.   Thompson, S.T.; Peterson, D.; Ho, D.; Papageorgopoulos, D. Perspective-The Next Decade of AEMFCs: Near-Term Targets to Accelerate Applied R&D. *J. Electrochem. Soc.* **2020**, *167*, 084514. [CrossRef]
7.   Liu, D.D.; Tao, L.; Yan, D.F.; Zou, Y.Q.; Wang, S.Y. Recent Advances on Non-precious Metal Porous Carbon-based Electrocatalysts for Oxygen Reduction Reaction. *ChemElectroChem* **2018**, *5*, 1775–1785. [CrossRef]
8.   Gewirth, A.A.; Varnell, J.A.; DiAscro, A.M. Nonprecious Metal Catalysts for Oxygen Reduction in Heterogeneous Aqueous Systems. *Chem. Rev.* **2018**, *118*, 2313–2339. [CrossRef]
9.   Osmieri, L.; Pezzolato, L.; Specchia, S. Recent trends on the application of PGM-free catalysts at the cathode of anion exchange membrane fuel cells. *Curr. Opin. Electrochem.* **2018**, *9*, 240–256. [CrossRef]
10. Shen, M.X.; Wei, C.T.; Ai, K.L.; Lu, L.H. Transition metal-nitrogen-carbon nanostructured catalysts for the oxygen reduction reaction: From mechanistic insights to structural optimization. *Nano Res.* **2017**, *10*, 1449–1470. [CrossRef]
11. Wood, K.N.; O'Hayre, R.; Pylypenko, S. Recent progress on nitrogen/carbon structures designed for use in energy and sustainability applications. *Energy Environ. Sci.* **2014**, *7*, 1212–1249. [CrossRef]
12. Thorum, M.S.; Hankett, J.M.; Gewirth, A.A. Poisoning the Oxygen Reduction Reaction on Carbon-Supported Fe and Cu Electrocatalysts: Evidence for Metal-Centered Activity. *J. Phys. Chem. Lett.* **2011**, *2*, 295–298. [CrossRef]
13. Kumar, Y.; Kibena-Põldsepp, E.; Kozlova, J.; Rähn, M.; Treshchalov, A.; Kikas, A.; Kisand, V.; Aruväli, J.; Tamm, A.; Douglin, J.C.; et al. Bifunctional Oxygen Electrocatalysis on Mixed Metal Phthalocyanine-Modified Carbon Nanotubes Prepared via Pyrolysis. *ACS Appl. Mater. Interfaces* **2021**, *13*, 41507–41516. [CrossRef] [PubMed]
14. Ratso, S.; Zitolo, A.; Käärik, M.; Merisalu, M.; Kikas, A.; Kisand, V.; Rähn, M.; Paiste, P.; Leis, J.; Sammelselg, V.; et al. Non-precious metal cathodes for anion exchange membrane fuel cells from ball-milled iron and nitrogen doped carbide-derived carbons. *Renew. Energy* **2021**, *167*, 800–810. [CrossRef]

15. Lilloja, J.; Kibena-Põldsepp, E.; Sarapuu, A.; Douglin, J.C.; Käärik, M.; Kozlova, J.; Paiste, P.; Kikas, A.; Aruväli, J.; Leis, J.; et al. Transition-Metal- and Nitrogen-Doped Carbide-Derived Carbon/Carbon Nanotube Composites as Cathode Catalysts for Anion-Exchange Membrane Fuel Cells. *ACS Catal.* **2021**, *11*, 1920–1931. [CrossRef]

16. Lilloja, J.; Kibena-Põldsepp, E.; Sarapuu, A.; Kodali, M.; Chen, Y.C.; Asset, T.; Käärik, M.; Merisalu, M.; Paiste, P.; Aruväli, J.; et al. Cathode Catalysts Based on Cobalt- and Nitrogen-Doped Nanocarbon Composites for Anion Exchange Membrane Fuel Cells. *ACS Appl. Energy Mater.* **2020**, *3*, 5375–5384. [CrossRef]

17. Lilloja, J.; Mooste, M.; Kibena-Põldsepp, E.; Sarapuu, A.; Zulevi, B.; Kikas, A.; Piirsoo, H.-M.; Tamm, A.; Kisand, V.; Holdcroft, S.; et al. Mesoporous iron-nitrogen co-doped carbon material as cathode catalyst for the anion exchange membrane fuel cell. *J. Power Sources Adv.* **2021**, *8*, 100052. [CrossRef]

18. Lilloja, J.; Kibena-Põldsepp, E.; Sarapuu, A.; Käärik, M.; Kozlova, J.; Paiste, P.; Kikas, A.; Treshchalov, A.; Leis, J.; Tamm, A.; et al. Transition metal and nitrogen-doped mesoporous carbons as cathode catalysts for anion-exchange membrane fuel cells. *Appl. Catal. B* **2022**, *306*, 121113. [CrossRef]

19. Sibul, R.; Kibena-Põldsepp, E.; Ratso, S.; Kook, M.; Sougrati, M.T.; Käärik, M.; Merisalu, M.; Aruväli, J.; Paiste, P.; Treshchalov, A.; et al. Iron- and Nitrogen-Doped Graphene-Based Catalysts for Fuel Cell Applications. *ChemElectroChem* **2020**, *7*, 1739–1747. [CrossRef]

20. Mooste, M.; Tkesheliadze, T.; Kozlova, J.; Kikas, A.; Kisand, V.; Treshchalov, A.; Tamm, A.; Aruväli, J.; Zagal, J.H.; Kannan, A.M.; et al. Transition metal phthalocyanine-modified shungite-based cathode catalysts for alkaline membrane fuel cell. *Int. J. Hydrogen Energy* **2021**, *46*, 4365–4377. [CrossRef]

21. Kisand, K.; Sarapuu, A.; Peikolainen, A.L.; Seemen, H.; Kook, M.; Käärik, M.; Leis, J.; Sammelselg, V.; Tammeveski, K. Oxygen Reduction on Fe- and Co-Containing Nitrogen-Doped Nanocarbons. *ChemElectroChem* **2018**, *5*, 2002–2009. [CrossRef]

22. Kisand, K.; Sarapuu, A.; Danilian, D.; Kikas, A.; Kisand, V.; Rähn, M.; Treshchalov, A.; Käärik, M.; Merisalu, M.; Paiste, P.; et al. Transition metal-containing nitrogen-doped nanocarbon catalysts derived from 5-methylresorcinol for anion exchange membrane fuel cell application. *J. Colloid Interface Sci.* **2021**, *584*, 263–274. [CrossRef] [PubMed]

23. Kisand, K.; Sarapuu, A.; Kikas, A.; Kisand, V.; Rähn, M.; Treshchalov, A.; Käärik, M.; Piirsoo, H.M.; Aruväli, J.; Paiste, P.; et al. Bifunctional multi-metallic nitrogen-doped nanocarbon catalysts derived from 5-methylresorcinol. *Electrochem. Comm.* **2021**, *124*, 106932. [CrossRef]

24. Mooste, M.; Kibena-Põldsepp, E.; Vassiljeva, V.; Kikas, A.; Käärik, M.; Kozlova, J.; Kisand, V.; Külaviir, M.; Cavaliere, S.; Leis, J.; et al. Electrospun Polyacrylonitrile-Derived Co or Fe Containing Nanofibre Catalysts for Oxygen Reduction Reaction at the Alkaline Membrane Fuel Cell Cathode. *ChemCatChem* **2020**, *12*, 4568–4581. [CrossRef]

25. Artyushkova, K.; Serov, A.; Rojas-Carbonell, S.; Atanassov, P. Chemistry of Multitudinous Active Sites for Oxygen Reduction Reaction in Transition Metal-Nitrogen-Carbon Electrocatalysts. *J. Phys. Chem. C* **2015**, *119*, 25917–25928. [CrossRef]

26. Kreek, K.; Sarapuu, A.; Samolberg, L.; Joost, U.; Mikli, V.; Koel, M.; Tammeveski, K. Cobalt-Containing Nitrogen-Doped Carbon Aerogels as Efficient Electrocatalysts for the Oxygen Reduction Reaction. *ChemElectroChem* **2015**, *2*, 2079–2088. [CrossRef]

27. Sokka, A.; Mooste, M.; Käärik, M.; Gudkova, V.; Kozlova, J.; Kikas, A.; Kisand, V.; Treshchalov, A.; Tamm, A.; Paiste, P.; et al. Iron and cobalt containing electrospun carbon nanofibre-based cathode catalysts for anion exchange membrane fuel cell. *Int. J. Hydrogen Energy* **2021**, *46*, 31275–31287. [CrossRef]

28. Jiang, M.H.; Yu, X.F.; Yang, H.Q.; Chen, S.L. Optimization Strategies of Preparation of Biomass-Derived Carbon Electrocatalyst for Boosting Oxygen Reduction Reaction: A Minireview. *Catalysts* **2020**, *10*, 21472. [CrossRef]

29. Kaur, P.; Verma, G.; Sekhon, S.S. Biomass derived hierarchical porous carbon materials as oxygen reduction reaction electrocatalysts in fuel cells. *Prog. Mater. Sci.* **2019**, *102*, 1–71. [CrossRef]

30. Li, Q.; Xu, D.; Ou, X.; Yan, F. Nitrogen-Doped Graphitic Porous Carbon Nanosheets Derived from In Situ Formed g-C_3N_4 Templates for the Oxygen Reduction Reaction. *Chem. Asian J.* **2017**, *12*, 1816–1823. [CrossRef]

31. Zhen, Z.H.; Jiang, Z.Q.; Tian, X.N.; Zhou, L.S.; Deng, B.L.; Chen, B.H.; Jiang, Z.J. Core@shell structured Co-CoO@NC nanoparticles supported on nitrogen doped carbon with high catalytic activity for oxygen reduction reaction. *RSC Adv.* **2018**, *8*, 14462–14472. [CrossRef] [PubMed]

32. Juvanen, S.; Sarapuu, A.; Vlassov, S.; Kook, M.; Kisand, V.; Kaarik, M.; Treshchalov, A.; Aruvali, J.; Kozlova, J.; Tamm, A.; et al. Iron-Containing Nitrogen-Doped Carbon Nanomaterials Prepared via NaCl Template as Efficient Electrocatalysts for the Oxygen Reduction Reaction. *ChemElectroChem* **2021**, *8*, 2288–2297. [CrossRef]

33. Eissa, A.A.; Peera, S.G.; Kim, N.H.; Lee, J.H. g-C_3N_4 templated synthesis of the Fe_3C@NSC electrocatalyst enriched with Fe-N-x active sites for efficient oxygen reduction reaction. *J. Mater. Chem. A* **2019**, *7*, 16920–16936. [CrossRef]

34. Zhang, G.; Lu, W.T.; Cao, F.F.; Xiao, Z.D.; Zheng, X.S. N-doped graphene coupled with Co nanoparticles as an efficient electrocatalyst for oxygen reduction in alkaline media. *J. Power Sources* **2016**, *302*, 114–125. [CrossRef]

35. Pan, F.P.; Jin, J.T.; Fu, X.G.; Liu, Q.; Zhang, J.Y. Advanced Oxygen Reduction Electrocatalyst Based on Nitrogen-Doped Graphene Derived from Edible Sugar and Urea. *ACS Appl. Mater. Interfaces* **2013**, *5*, 11108–11114. [CrossRef]

36. Liu, Q.; Duan, Y.X.; Zhao, Q.P.; Pan, F.P.; Zhang, B.; Zhang, J.Y. Direct Synthesis of Nitrogen-Doped Carbon Nanosheets with High Surface Area and Excellent Oxygen Reduction Performance. *Langmuir* **2014**, *30*, 8238–8245. [CrossRef]

37. Enterria, M.; Figueiredo, J.L. Nanostructured mesoporous carbons: Tuning texture and surface chemistry. *Carbon* **2016**, *108*, 79–102. [CrossRef]

38. Li, X.H.; Kurasch, S.; Kaiser, U.; Antonietti, M. Synthesis of Monolayer-Patched Graphene from Glucose. *Angew. Chem. Int. Ed.* **2012**, *51*, 9689–9692. [CrossRef]
39. Tian, Y.H.; Xu, L.; Bao, J.; Qian, J.C.; Su, H.N.; Li, H.M.; Gu, H.D.; Yan, C.; Li, H.N. Hollow cobalt oxide nanoparticles embedded in nitrogen-doped carbon nanosheets as an efficient bifunctional catalyst for Zn-air battery. *J. Energy Chem.* **2019**, *33*, 59–66. [CrossRef]
40. Asset, T.; Atanassov, P. Iron-Nitrogen-Carbon Catalysts for Proton Exchange Membrane Fuel Cells. *Joule* **2020**, *4*, 33–44. [CrossRef]
41. Deng, D.H.; Yu, L.; Chen, X.Q.; Wang, G.X.; Jin, L.; Pan, X.L.; Deng, J.; Sun, G.Q.; Bao, X.H. Iron Encapsulated within Pod-like Carbon Nanotubes for Oxygen Reduction Reaction. *Angew. Chem. Int. Ed.* **2013**, *52*, 371–375. [CrossRef] [PubMed]
42. Jiang, W.J.; Gu, L.; Li, L.; Zhang, Y.; Zhang, X.; Zhang, L.J.; Wang, J.Q.; Hu, J.S.; Wei, Z.D.; Wan, L.J. Understanding the High Activity of Fe-N-C Electrocatalysts in Oxygen Reduction: Fe/Fe$_3$C Nanoparticles Boost the Activity of Fe-N-x. *J. Am. Chem. Soc.* **2016**, *138*, 3570–3578. [CrossRef] [PubMed]
43. Sgarbi, R.; Kumar, K.; Jaouen, F.; Zitolo, A.; Ticianelli, E.A.; Maillard, F. Oxygen reduction reaction mechanism and kinetics on M-N(x)C(y)and M@N-C active sites present in model M-N-C catalysts under alkaline and acidic conditions. *J. Solid State Electrochem.* **2021**, *25*, 45–56. [CrossRef]
44. Thommes, M.; Kaneko, K.; Neimark, A.V.; Olivier, J.P.; Rodriguez-Reinoso, F.; Rouquerol, J.; Sing, K.S.W. Physisorption of gases, with special reference to the evaluation of surface area and pore size distribution (IUPAC Technical Report). *Pure Appl. Chem.* **2015**, *87*, 1051–1069. [CrossRef]
45. Liang, H.W.; Zhuang, X.D.; Bruller, S.; Feng, X.L.; Mullen, K. Hierarchically porous carbons with optimized nitrogen doping as highly active electrocatalysts for oxygen reduction. *Nat. Commun.* **2014**, *5*, 4973. [CrossRef] [PubMed]
46. Goldie, S.J.; Jiang, S.; Coleman, K.S. Cobalt nanoparticle catalysed graphitization and the effect of metal precursor decomposition temperature. *Mater. Adv.* **2021**, *2*, 3353–3361. [CrossRef]
47. Jia, Q.; Ramaswamy, N.; Tylus, U.; Strickland, K.; Li, J.; Serov, A.; Artyushkova, K.; Atanassov, P.; Anibal, J.; Gumeci, C.; et al. Spectroscopic insights into the nature of active sites in iron–nitrogen–carbon electrocatalysts for oxygen reduction in acid. *Nano Energy* **2016**, *29*, 65–82. [CrossRef]
48. Biesinger, M.C.; Payne, B.P.; Grosvenor, A.P.; Lau, L.W.M.; Gerson, A.R.; Smart, R.S. Resolving surface chemical states in XPS analysis of first row transition metals, oxides and hydroxides: Cr, Mn, Fe, Co and Ni. *Appl. Surf. Sci.* **2011**, *257*, 2717–2730. [CrossRef]
49. Bertóti, I.; Mohai, M.; László, K. Surface modification of graphene and graphite by nitrogen plasma: Determination of chemical state alterations and assignments by quantitative X-ray photoelectron spectroscopy. *Carbon* **2015**, *84*, 185–196. [CrossRef]
50. Susi, T.; Pichler, T.; Ayala, P. X-ray photoelectron spectroscopy of graphitic carbon nanomaterials doped with heteroatoms. *Beilstein J. Nanotechnol.* **2015**, *6*, 177–192. [CrossRef]
51. Ratso, S.; Kruusenberg, I.; Sarapuu, A.; Kook, M.; Rauwel, P.; Saar, R.; Aruvali, J.; Tammeveski, K. Electrocatalysis of oxygen reduction on iron- and cobalt-containing nitrogen-doped carbon nanotubes in acid media. *Electrochim. Acta* **2016**, *218*, 303–310. [CrossRef]
52. Bard, A.J.; Faulkner, L.R. *Electrochemical Methods*, 2nd ed.; Wiley: New York, NY, USA, 2001.
53. Davis, R.E.; Horvath, G.L.; Tobias, C.W. The solubility and diffusion coefficient of oxygen in potassium hydroxide solutions. *Electrochim. Acta* **1967**, *12*, 287–297. [CrossRef]
54. Lide, D.R. *CRC Handbook of Chemistry and Physics*; CRC Press: Boca Raton, FL, USA, 2001.
55. Mineva, T.; Matanovic, I.; Atanassov, P.; Sougrati, M.T.; Stievano, L.; Clemancey, M.; Kochem, A.; Latour, J.M.; Jaouen, F. Understanding Active Sites in Pyrolyzed Fe-N-C Catalysts for Fuel Cell Cathodes by Bridging Density Functional Theory Calculations and Fe-57 Mossbauer Spectroscopy. *ACS Catal.* **2019**, *9*, 9359–9371. [CrossRef]
56. Zitolo, A.; Ranjbar-Sahraie, N.; Mineva, T.; Li, J.K.; Jia, Q.Y.; Stamatin, S.; Harrington, G.F.; Lyth, S.M.; Krtil, P.; Mukerjee, S.; et al. Identification of catalytic sites in cobalt-nitrogen-carbon materials for the oxygen reduction reaction. *Nat. Commun.* **2017**, *8*, 957. [CrossRef]
57. Zagal, J.H.; Specchia, S.; Atanassov, P. Mapping transition metal-MN4 macrocyclic complex catalysts performance for the critical reactivity descriptors. *Curr. Opin. Electrochem.* **2021**, *27*, 100683. [CrossRef]
58. He, Y.H.; Hwang, S.; Cullen, D.A.; Uddin, M.A.; Langhorst, L.; Li, B.Y.; Karakalos, S.; Kropf, A.J.; Wegener, E.C.; Sokolowski, J.; et al. Highly active atomically dispersed CoN$_4$ fuel cell cathode catalysts derived from surfactant-assisted MOFs: Carbon-shell confinement strategy. *Energy Environ. Sci.* **2019**, *12*, 250–260. [CrossRef]
59. Huang, K.; Zhang, L.; Xu, T.; Wei, H.H.; Zhang, R.Y.; Zhang, X.Y.; Ge, B.H.; Lei, M.; Ma, J.Y.; Liu, L.M.; et al. −60 °C solution synthesis of atomically dispersed cobalt electrocatalyst with superior performance. *Nat. Commun.* **2019**, *10*, 606. [CrossRef]
60. Strickland, K.; Miner, E.; Jia, Q.; Tylus, U.; Ramaswamy, N.; Liang, W.; Sougrati, M.-T.; Jaouen, F.; Mukerjee, S. Highly active oxygen reduction non-platinum group metal electrocatalyst without direct metal-nitrogen coordination. *Nat. Commun.* **2015**, *6*, 7343. [CrossRef]
61. Yang, Y.; Zeng, R.; Xiong, Y.; DiSalvo, F.J.; Abruna, H.D. Cobalt-Based Nitride-Core Oxide-Shell Oxygen Reduction Electrocatalysts. *J. Am. Chem. Soc.* **2019**, *141*, 19241–19245. [CrossRef]
62. Tylus, U.; Jia, Q.Y.; Strickland, K.; Ramaswamy, N.; Serov, A.; Atanassov, P.; Mukerjee, S. Elucidating Oxygen Reduction Active Sites in Pyrolyzed Metal-Nitrogen Coordinated Non-Precious-Metal Electrocatalyst Systems. *J. Phys. Chem. C* **2014**, *118*, 8999–9008. [CrossRef]